

Crystalline SiSe_2 and $\text{Si}_x\text{Se}_{1-x}$ glasses: Syntheses, glass formation, structure, phase separation, and Raman spectra

J. E. Griffiths, M. Malyj, G. P. Espinosa, and J. P. Remeika

AT&T Bell Laboratories, Murray Hill, New Jersey 07974

(Received 2 February 1984; revised manuscript received 17 August 1984)

Crystalline SiSe_2 and a series of $\text{Si}_x\text{Se}_{1-x}$ clear yellow-orange glasses ($0.33 < x \leq 0.4$) were synthesized and studied by Raman spectroscopy. Spectra of crystals were analyzed in terms of the known crystal structure of SiSe_2 whereas for the glasses a new cross-linked chain-cluster model (CLCC) is proposed and is the basis for extensive spectral analysis. Extended chain-only and random-network models are inconsistent with the data. The CLCC model is characterized by well-defined chains of edge-sharing (SiSe_4) tetrahedra, as in the crystal, which are cross-linked via corner-sharing (SiSe_4) tetrahedra to form very large, highly viscous inorganic polymers. The structure has extensive medium-range order and provides for a self-consistent mechanism for transition to nonstoichiometric glasses in the range SiSe_2 to Si_2Se_3 . The smooth transition to various compositions is readily monitored through spectral changes in the Si-Se vibrational stretching region ($150\text{--}300\text{ cm}^{-1}$) and in the region of the collective modes at lower frequency ($0\text{--}150\text{ cm}^{-1}$).

I. INTRODUCTION

Crystalline silicon diselenide, *c*- SiSe_2 , has a very different structure from that of the high-temperature monoclinic form of its chemical analog germanium diselenide, GeSe_2 . A striking feature of the latter is its two-dimensional micaceous layer structure¹ in which chains of corner-sharing (GeSe_4) tetrahedra² are periodically cross linked with edge-sharing (GeSe_4) units. The layers are held together via weak van der Waals forces. The silicon analog, by contrast, is made up of semi-infinite chains of edge-sharing (SiSe_4) tetrahedra with the parallel chains being held in place through van der Waals forces. There are no corner-sharing tetrahedral structural units in the single crystal.³⁻⁸

The ability of germanium diselenide to form dark red glasses over an extensive range of compositions around the nominal GeSe_2 stoichiometry by rapid quenching from the melt is well documented and quite well understood.^{9,10} The basic structural units in the glass are thought to be composed of two-dimensional raftlike fragments of the crystal, which are initially formed by fragmentation on melting at high temperature and whose structures are frozen in the quenching process. Important features in the structure are considerable medium-range order within the partially polymerized clusters and the presence of cluster growth limiting Se-Se and Ge-Ge wrong bonds.¹¹⁻¹³

By contrast, the glass-forming tendency of silicon diselenide is not as well studied or understood. Although the structures of crystalline SiSe_2 (Ref. 8) and GeSe_2 (Ref. 1) are quite different, they are similar chemically and the information available from our earlier studies of GeSe_2 , GeS_2 , and $\text{GeS}_x\text{Se}_{2-x}$ glasses^{11,13} allows us to speculate in a reasonable way on what to expect with SiSe_2 . There is little actually known about SiSe_2 . Pure congruently melting crystals of SiSe_2 [melting point (mp) 970°C] have been prepared^{14,15} and the structure was determined.³⁻⁸ Only

a brief mention of a glass phase has appeared,¹⁶ along with preliminary data from a cursory examination of the infrared spectrum of crystalline material.⁷ More recently and during the course of the present work a study of SiSe_2 glass has been published.¹⁷ The present work, however, indicates a different microscopic structure of the SiSe_2 glass is likely.

The work of Tenhover *et al.*¹⁷ on SiSe_2 and $\text{Si}_x\text{Se}_{1-x}$ ($0.30 < x < 0.4$) glasses introduces the idea of a basic orientationally disordered or randomly packed structure of extended $(\text{SiSe}_2)_n$ chains. To explain their spectral data for the SiSe_2 glass itself they assigned the so-called " A_1^B " band to a $\text{Si}_2(\text{Se}_{1/2})_8$ bitetrahedral cluster unit. In the nonstoichiometric glasses, they introduced a second kind of Si_2Se_3 "cluster" and concluded that glasses with $0.333 < x \leq 0.400$ are composed of fractions of SiSe_2 and Si_2Se_3 "glassy compounds." They also suggested that Si_2Se_3 may in fact exist as quasi-one-dimensional units $(\text{Se}_3\text{-Si-Si-Se}_3)_n$. The basic concept of one-dimensional chains of this type led them to unusual valence arguments to describe the role of silicon in such structures. This was unnecessary for the case of the Si_2Se_3 composition because the structure is more likely to exist as a three-dimensional network of the type already established for Si_2Te_3 . In such structures, silicon assumes its normal +4 valency. In contrast to these earlier conclusions¹⁷ we have found that a more complicated model is necessary to account for the complex spectra observed for $\text{Si}_x\text{Se}_{1-x}$ glasses in the range $0.333 < x < 0.400$.

The present work represents a systematic study of the selenium-silicon system and covers several facets of the problem, including crystalline SiSe_2 and $\text{Si}_x\text{Se}_{1-x}$ glasses. Section II concerns the structure and Raman spectra of crystalline SiSe_2 . The equilibrium phase relationships of $\text{Si}_x\text{Se}_{1-x}$ covering the range from pure selenium ($x=0$) to the SiSe stoichiometric compound are discussed in Sec. III. The three glass models are presented in Sec. IV. Experimental details are given in Sec. V and results are

shown in Sec. VI. Section VII contains discussion and conclusions.

II. CRYSTALLINE SiSe_2 AND VIBRATIONAL SYMMETRY COORDINATES

The structure of single-crystal SiSe_2 was determined first by Weiss and Weiss.⁴⁻⁸ The space group is orthorhombic D_{2h}^{26} (*Ibam*) and the cell dimensions (273 K) are $a=9.669\pm 0.003$, $b=5.998\pm 0.002$, and $c=5.851\pm 0.002$ Å.⁸ There are four empirical SiSe_2 units per unit cell and two per primitive cell leading to a density of 3.640 g cm^{-3} at 273 K (observed value $3.63\pm 0.03 \text{ g cm}^{-3}$).¹⁸ Figure 1 shows the spatial relationships of some of the silicon diselenide chains in two unit cells.

For this structure the irreducible representation of internal symmetry coordinates is given by group theory¹⁹ as

$$\begin{aligned} \Gamma = & 2A_g^{(R)} + 3B_{1g}^{(R)} + 2B_{2g}^{(R)} + 2B_{3g}^{(R)} + B_{1u}^{(IR)} + 2B_{2u}^{(IR)} \\ & + 2B_{3u}^{(IR)} + A_u^{(\text{inactive})} + B_{1u}^{(\text{acoustic})} \\ & + B_{2u}^{(\text{acoustic})} + B_{3u}^{(\text{acoustic})}. \end{aligned}$$

The nine gerade modes are Raman active (R) and there are five infrared-active (IR) ungerade modes, leaving one inactive mode and three acoustic modes that are inactive in the infrared and Raman spectra. Figure 2 shows the various symmetry coordinates in a plan representation (*ab* plane). The *c* axis is out of the plane of the figure. The selenium atoms, represented by solid circles, are above the plane of the silicon atoms, and those represented by open circles are below the same plane. Arrows denote the directions of atomic motion in the *ab* plane. Plus and minus signs indicate motions of appropriate atoms out of and into the plane of the diagram, respectively. Thus the $\nu_1 A_g$ mode shows the symmetric SiSe_4 stretching coordinate which would correspond to the totally symmetric ν_1 , (a_1) mode of an isolated SiBr_4 -type molecule. In this case, however, the tetrahedra share edges which change the nature of the atomic motions from directly along the bond axes to one in which the selenium atoms move simultaneously away from each other and from the nearest silicon atoms symmetrically.

In B_{1g}, ν_3 , the silicon atoms in the *c*-axis chains centered on the edges of the unit cell move in a direction out

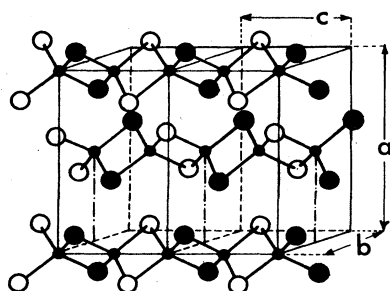


FIG. 1. Two unit cells of *c*- SiSe_2 showing some of the linear chains of edge-sharing (SiSe_4) tetrahedra. Small circles are silicon; large, open and solid circles are selenium in alternating *ab* planes.

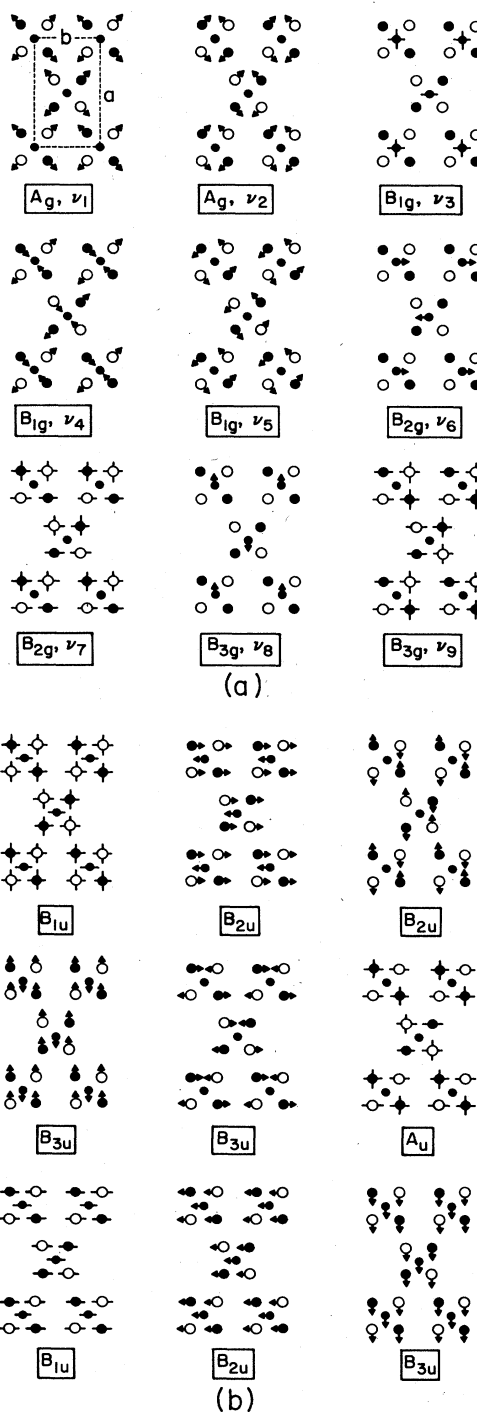


FIG. 2. (a) Gerade symmetry coordinates for *c*- SiSe_2 . Long axes of chains of edge-sharing tetrahedra are normal to the plane for the diagram. Silicon atoms are the smallest solid circles. (b) Ungerade symmetry coordinates for *c*- SiSe_2 . Long axes of chains of edge-sharing tetrahedra are normal to the plane for the diagram. Silicon atoms are the smallest solid circles.

of the *ab* plane in phase with one another. The silicon atoms in the body-center chains move in the opposite direction, into the *ab* plane.

The observed Raman spectrum of crystalline SiSe_2 should consist of nine bands. Data to be shown in Sec. V

will confirm this expectation. It is useful to point out, however, that this vibrational analysis in terms of idealized symmetry coordinates is a first-order approximation only. The actual motions of the atoms in the normal coordinates will be considerably more complex and in general will be an admixture of these symmetry coordinates. The present treatment will be adequate for our purposes which is directed to a better understanding of the structures of the $\text{Si}_x\text{Se}_{1-x}$ glasses.

III. PHASE RELATIONSHIPS IN THE Si-SE SYSTEM

There is a limited amount of information available about the stable phases at equilibrium in the silicon-selenium system. Even in the absence of a complete study of the phase diagram for the system, a few experiments and some speculative reasoning allow us to propose a tentative diagram. Part of the problem in actually determining the complete diagram experimentally rests in the chemical and physical properties of the two components, Si and Se, their reactivity with sample containers at high temperatures, and the need to work in the complete absence of air and moisture.

Three compositions in the system are well known: Si (mp 1420°C),²⁰ Se (mp 221.2°C),²¹ and the congruently melting compound SiSe_2 (mp 970°C).⁷ Less well characterized is the compound SiSe which is most probably incongruently melting.¹⁵ A third nonstoichiometric binary compound, Si_2Se_3 must be considered by analogy with Si_2Te_3 , the only known compound in the Si-Te system. Evidence will be presented later in this work which exempts Si_2Se_3 from consideration as a stable compound.

Figure 3 shows our proposed phase diagram in which

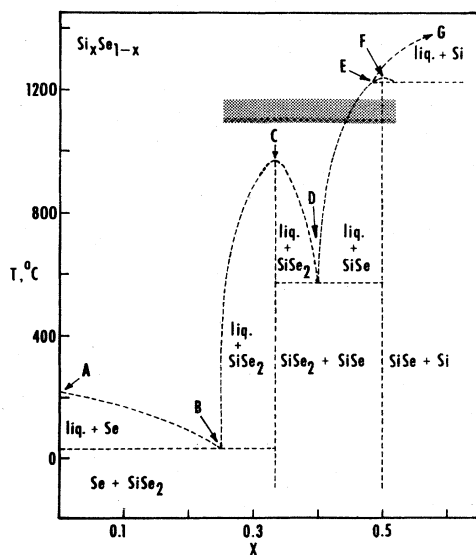


FIG. 3. Proposed equilibrium phase diagram of the Si-Se system for $0 \leq x \leq 0.66$. Identifying letters (A–G) are discussed in the text. Cross-hatched area represents fixative temperature (1100°C) and composition range ($0.250 \leq x \leq 0.525$) of water quench experiments.

important composition-temperature points are labeled with letters. Points A, C, and G are well established with respect to temperature and composition. Point G is off the diagram at $X=1.0$ and represents pure silicon (mp 1420°C).²⁰ There is no reason to propose a stable binary compound between points A and C and therefore a simple eutectic at B is expected. The temperature and composition of B are unknowns but are expected at $T < 220^\circ\text{C}$ and $x \leq 0.3$.

Points D, E, and F are extremely important because they refer to the Si_2Se_3 and SiSe compounds. As drawn, Si_2Se_3 is not a stable identifiable compound whereas SiSe is incongruently melting with decomposition, presumably according to the reaction,



All attempts to form Si_2Se_3 from the elements were unsuccessful. Quenching of melts having compositions between SiSe_2 and Si_2Se_3 resulted in clear glasses which on analysis of their Raman spectra led to the conclusion that point D at $x=0.40$ was in fact a eutectic point. The composition of point D seems certain but the temperature is not. By definition $T_D < T_C$. For all experiments in the range $0.400 \leq x < 0.525$, two phases, a clear amber liquid, which ultimately forms a glass, and a dark solid, were apparently in equilibrium. Quenching led to a mass having progressively less glass and more solid as x approached 0.5. Thus, the liquidus curve DE is probably more steeply rising than drawn with $T_E > 1100^\circ\text{C}$, the fixative temperature of all of the melt-quench experiments. The existence of SiSe , point F, is assumed. Attempts to prepare and identify such a compound from stoichiometric mixtures of the elements were not successful. In such attempts, one could generally observe and identify small crystals of pure silicon deposited from the vapor phase onto the walls of the tubes used to contain the samples. This, we believe, represents the decomposition of SiSe according to Eq. (1). The composition and temperature of points E and F are not known with certainty. Both T_E and T_F , however, are greater than 1100°C.

Thus, the basic features of the phase diagram are known even though there are some uncertainties about exact compositions and temperatures of some of the important points. The proposed diagram more closely resembles that previously determined for the Ge-Se (Refs. 9 and 22) system than it does the Si-Te (Refs. 23–26) one. The cross-hatched area shown in Fig. 3 is the composition range over which data were obtained in the present study.

IV. MODELS FOR $\text{Si}_x\text{Se}_{1-x}$ GLASSES

There is almost unlimited scope in developing models for glass structures. These include completely random networks at one extreme and highly regular structures with atomic periodicity approaching that of the crystalline phase at the other. The random-network models have enjoyed considerable acceptance for a long time, but are gradually losing favor for some glasses as new kinds of data from more powerful experimental techniques are focused on the problem. Currently, random-network models, which are characterized by a lack of medium-

range atomic order, but retain nearest-neighbor short-range order, are inadequate to account for the ever increasing amount of structural information that has become available for many glasses. Thus, random-network models should more realistically become the models of last resort.

To develop a satisfactory model for the range of composition that readily forms glasses in the Si-Se system, it is useful to start with crystalline SiSe_2 and to make a basic assumption about the fate of the crystalline structure on melting. Adequate thermal energy is available to destroy the cohesive forces holding the chains parallel to each other and to randomize the orientation of the chain axes with respect to each other. Furthermore, chain length reduction via fragmentation at 1100°C , the fixative temperature²⁷ of the experiments done in this work, is also expected. Several things can occur.

After fragmentation the chains can retain their integrity, in which case each can be characterized as a free radical with one or more unpaired electrons, presumably localized at the chain ends. This is the radical-chain model. Provided that the rate of recombination of chains is slow relative to the quenching rate, the glass, after quenching, should have a high concentration of unpaired spins. In the highly viscous glass state, the recombination rate leading to the formation of longer chains and ultimately to the crystalline phase at higher temperatures, will be diffusion controlled. Thus, measurements on freshly prepared samples of SiSe_2 glass should yield very high spin densities. Measurements of this type have been done and very low spin densities of order 10^{15} spin/g were reported.¹⁵ This can be compared to a value of 10^{18} spins/g for $(\text{SiO})_n$ glasses.¹⁵ It seems reasonable, then, to eliminate the radical-chain model from further consideration.

A second but somewhat similar model based on a chain structure can also be proposed. In this case, individual chains, whose average length is determined by the fixative temperature, can be chemically stabilized through chain-terminating seleno-siliconyl groups of the type shown in Fig. 4(b). This is structurally and chemically satisfying in that all valence requirements are satisfied, no unusual highly strained bond angles are required, and the basic chain structure of edge-sharing tetrahedra is retained. The troublesome aspect of this model is inclusion of well-defined π bonding in the $\text{Si}=\text{Se}$ chain-terminating group and a planar bonding configuration not generally favored by silicon. An exception can be found in the unstable $\text{OSi}=\text{S}$ triatomic species isolated in a low-temperature argon matrix.²⁸ Tetrahedral or octahedral coordination is normal. If this chain model is important in the glass phase, the Raman spectrum should contain spectral bands in common with the crystal, without a lot of extra bands. Also, the relative intensities of the glass and crystal bands should scale appropriately. In addition, bands due to vibrations of the $\text{Si}=\text{Se}$ chain end groups should be detectable. Based on observed values for related molecules containing double-bonded linkages [OSiS (Ref. 28), PSBr_3 (Ref. 29), and POBr_3 (Ref. 30)], one can expect a frequency for $>\text{Si}=\text{Se}$ to be in the $450\text{--}550\text{-cm}^{-1}$ range. Because of the extended chain separating the end groups and expected minimal chain to chain interactions, the

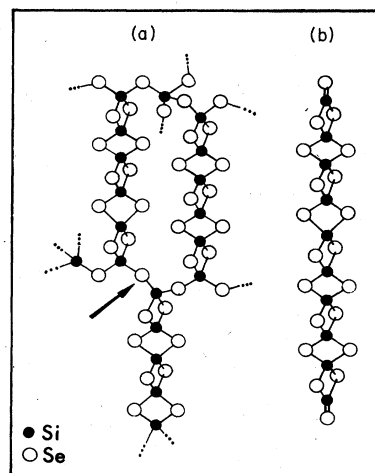


FIG. 4. Structural models of SiSe_2 glass. (a) Cross-linked chain-cluster model; (b) seleno-siliconyl terminated extended-chain model.

$>\text{Si}=\text{Se}$ band is also expected to be reasonably narrow. There is little if any spectral evidence favoring this model.

A third, the cross-linked chain-cluster (CLCC) model, which is physically and chemically appealing, is shown in Fig. 4(a). In this structure, edge-sharing (SiSe_4) tetrahedral units in well-defined chains are retained and individual chains are linked to each other via corner-sharing bonds. The latter type of bonding initially forms in the melt as a result of interactions between chain ends. It is apparent from the model of Fig. 4(a) that very large molecular structures can result and this would be reflected in giant viscosities even at elevated temperatures. Information will be presented later showing that the viscosity of a SiSe_2 melt at 1100°C is so great that the mass will not flow under the force of gravity. This is in sharp contrast to GeSe_2 melts which flow readily at significantly lower temperatures.

The inclusion of corner-sharing tetrahedral bonding in the CLCC model leads to significantly higher free volume in the region between edge-sharing chains than one might expect for a model containing only extended linear chains. In this regard it is useful to consider several linear organic polymers such as polyethylene, polypropylene, polypentene, and polystyrene, the last of which has its glass transition temperature well above room temperature, while the others have T_g values below. The densities of the crystalline and amorphous polymers are well known. Noncrystalline organic polymers at $T < T_g$ are considered to be glasses. At $T > T_g$ they are rubbers.³¹ In general, the ratio of crystalline to amorphous polymer densities fall in the narrow range of 1.08 (polystyrene) to 1.18 (polyethylene) and the average is 1.13.³¹ Selected values are collected in Table I.

The smallest value is for polystyrene, which is the one example having T_g higher than room temperature. The corresponding densities for SiSe_2 [$\rho_c = 3.64 \text{ g/cm}^3$; $\rho_g = 2.95 \text{ g/cm}^3$ (Refs. 8 and 16)] are also known and give a density ratio of $\rho_c/\rho_g = 1.23$. The only organic polymer with a comparable value (1.25) is polymethylene oxide,

TABLE I. Density ratios of crystalline and amorphous linear polymers (Ref. 31).

Material	ρ_c^a Crystalline g/cm ³	ρ_a^a Amorphous g/cm ³	T_g (K)	ρ_c/ρ_a^a
Polyethylene	1.00	0.85	153	1.18
Polypropylene	0.95	0.85	253	1.12
Polybutene	0.95	0.86	228	1.10
Polypentene	0.94	0.86	221	1.09
Polystyrene	1.13	1.05	373	1.08
Polymethylene oxide	1.54	1.25	190	1.25
SiSe ₂	3.64	2.95	735	1.23

^aValues are for room temperature.

and two factors make contributions to that high value. First, this polymer has a low T_g and like the other linear polymers listed in Table I, room-temperature density ratios are higher when $T > T_g$. Secondly, the $(-\text{CH}_2\text{OCH}_2\text{O}-)_n$ bonding structure is highly kinked and is likely to have greater free volume than it would have if it were to exist as linear extended chains.

The temperature dependence of the viscosity of long-chain organic polymers is predictable in the range T_g to $3T_g$.³¹ Increasing T/T_g from 1 to 2 and for chain lengths of about 10^6 molecular repeat units, the viscosity will fall about 11 orders of magnitude. At that point, T is above the melting point T_m of the crystalline polymer. When bulk GeSe₂ is heated (1175 K) to $T/T_g = 1.76$, well above T_m (1013 K), the melt flows freely. The structural units in the melt are thought to be raftlike,¹¹ containing the order of 1000 atoms. When SiSe₂ is heated to 1373 K ($T_m = 1243$ K, $T/T_g = 1.87$), the melt is so viscous that it will not flow in an inverted sealed tube over a period of 24 h. It would seem, therefore, that extended-chain models or raftlike models for SiSe₂ melts are unlikely. More likely is a model involving giant molecules with extensive cross linking. Thus both viscosity and density considerations favor the CLCC model over those involving only extended chains.

The main feature of the CLCC model, aside from accounting for the observed giant viscosities and the large density ratio, is the retention of the basic idea of edge-sharing tetrahedral chains and the lack of unrealistic bond distances and angles. Thus one preserves the concept of a high degree of medium-range order in one dimension and to a lesser extent in the other two dimensions. This is in sharp contrast to the extended-chain models which invoke medium-range order in one dimension only, with the longitudinal chain axes randomly distributed in space. Two other factors are also important. The presence of chain branching points via corner-sharing bonding means that the Raman spectrum should contain observable bands not associated with edge-sharing chains. Thus the spectrum of a stoichiometric glass will be significantly more complicated than a band-broadened version of the crystalline spectrum. Secondly, this structural model lends itself to the insertion of silicon atoms or equivalently the elimination of selenium atoms to allow a smooth conversion of the structure from that of SiSe₂ to that corresponding to the Si₂Se₃ composition. This covers the complete compo-

sition range of glasses that readily form in actual experiments.

Consider, first, the selenium atoms bridging the upper left chain to the lower middle chain in Fig. 4(a). This point is identified by an arrow. If this selenium atom is eliminated, the adjacent silicon atoms can reform as a Si-Si bond, producing a dumbbell-type structural unit much like that observed in Si₂Te₃.^{32,33} On the basis of molecular models such dumbbells should appear, especially near the SiSe₂ stoichiometry, in pairs so that only minimal strain and a slight distortion of the local structure obtains. Further elimination of selenium allows the Si-Si bonds to thread their way throughout the glass with only minor distortion of the local structure. As the composition approaches $x = 0.40$ or Si₂Se₃, the structure becomes saturated with Si-Si bonding and forms a natural cutoff for glass formation. Further increases in silicon content to form, for example, silicon-monoselenide-type glasses or amorphous solids, must proceed by a different mechanism.³⁴ The initial restriction of introducing Si-Si bonds in localized pairs to relieve consequential stress near the SiSe₂ composition suggests the need for a critical silicon doping concentration to be present for the corresponding glass structure to be energetically favored over phase separation. Experimentally, there is a small composition range $0.333 < x < 0.345$ where glasses are difficult to prepare and the tendency for phase separation becomes strong, a feature that has attracted considerable attention in near stoichiometric metallic glasses.³⁵ Moreover, earlier work with Ge-Se alloys⁹ demonstrated a maximum in the curve of glass-forming difficulty at the stoichiometric GeSe₂ composition compared with those compositions on either side.

All of the data to be presented in later sections support the CLCC model for silicon-selenium glasses in the composition range $0.333 < x < 0.400$. In this composition range, an additional attractive feature of our cross-linked chain-cluster model (CLCC) is the ability it has to accommodate the gradual and continuous introduction of disorder (Si-Si bonding) into a structure characterized by an initial high degree of medium-range order.

V. EXPERIMENTAL PART

A. Preparation of glass and crystalline phases

In typical glass preparations, 1.0 g lots of finely ground silicon (99.999%) and previously vacuum-melted selenium

(99.999%) were weighted in appropriate mole ratios $\text{Si}_x\text{Se}_{1-x}$ ($0.250 \leq x \leq 0.525$) and sealed under vacuum (10^{-3} – 10^{-4} Torr) in 8-cm fused silica tubes (6 mm inner diameter). The various tubes were gradually heated to 1100°C over a period of 8 h, then held at this temperature for times varying from 24 to 72 h. Rapid melt-quenching was performed by dropping the hot tubes directly from the furnace into water.

The results, to be reported in Sec. VI, show that products depend on the initial composition of the silicon-selenium mixture. This is to be expected from Fig. 3. Depending on the initial composition the following materials were produced: yellow-orange glasses ($x=0.333$, $0.345 \leq x < 0.38$), orange-yellow glasses ($0.38 < x \leq 0.400$), phase-separated cloudy yellow-orange glasses ($0.338 < x < 0.345$), and phase-separated orange-yellow glasses ($0.400 < x < 0.525$). In all of the phase-separated cases listed here, a clearly defined boundary is apparent between the lower translucent glass phase and an upper opaque phase. For the composition range $0.400 < x < 0.410$, the lower glass phase was contaminated with small dark crystalline platelets and whiskers. Raman analysis produced no detectable spectrum attributable to these particles.

Crystalline SiSe_2 was prepared in several ways from the melt-quenched samples described above. Sealed samples with $x=0.333$ were reheated to 1100°C for periods of 4 h followed by slow cooling ($8^\circ\text{C}/\text{h}$) to 960°C , a few degrees below the known melting point of SiSe_2 (970°C). The samples were held at this temperature for 4 days followed by further slow cooling to 910°C . The samples were then allowed to cool more rapidly by shutting off current to the furnace. Fibrous white crystal were evident.

Alternatively, hot samples were cooled from 1120 to 560°C at a rate of $5^\circ\text{C}/\text{h}$ followed by a more rapid cooling to room temperature. For a sample with $x=0.345$, a myriad of white fibrous crystals of SiSe_2 protruded from a background mass of yellow-orange glass. Raman spectral analysis indicated that the crystalline SiSe_2 aggregates were embedded in a glassy matrix richer in silicon than that of the initial composition.

With initial composition $x=0.400$ or 0.500 , however, wetting of the interior silica surface and possibly reaction of the silica tube with its contents resulted in tube fracture during slow cooling. Subsequent reaction with atmospheric water vapor produced the dangerously toxic compound H_2Se as a volatile product (bp -42°C). This effect is less severe at $x=0.400$.

The high reactivity of all of the materials with water vapor in air precluded a convincing characterization of the samples by differential thermal analysis (DTA) or differential scanning calorimetry (DSC) techniques. The samples are considerably more reactive than the data of Emons and Theisen¹⁵ would suggest and therefore characterizing materials whose integrity could not be guaranteed was not pursued.

B. Raman spectra

All samples were studied in their as-prepared state without opening the vitreous silica tubes. One of the problems with this arises from the physical condition of the external surfaces of the sample tubes following

quenching in water from 1100°C . Generally, the tubes were cloudy from devitrification or reaction of silica with water forming a rough crusty surface which badly scattered the incoming laser light beam. Immersing these sample tubes in another Pyrex tube containing a transparent liquid (xylene) allowed the incoming laser beam to penetrate to the sample and the Raman-scattered light to escape without appreciable attenuation or diffuse scattering by the imperfect sample-tube surface. No detectable Raman bands from the index matching liquid, the spectrum of which was well known, were observed.

Raman excitation was done using the 6471 or 6764 Å lines from a Spectra Physics model 171 krypton ion laser. Experiments were done using either horizontal or vertical polarization of the laser beam depending on whether the samples were opaque or transparent to the incident light. For opaque samples, a backscattering geometry was used. For transparent samples (glasses), a conventional 90° scattering geometry was used. Scattered light was analyzed with an Instruments S.A. U-1000 double monochromator fitted with 1200 g/mm or 1800 g/mm plane Jobin-Yvon holographic gratings and a Hammamatsu R-928 photomultiplier with associated photon counting electronics. A Data General Eclipse S/130 minicomputer was used to control all aspects of the apparatus, experiments, and data processing. Spectral slit widths (SSW) varied from less than 1 cm^{-1} to as large as 3 cm^{-1} , depending on the nature of individual samples. Typically, 2 cm^{-1} was selected for the SSW.

VI. RESULTS AND DISCUSSION

A. Crystalline SiSe_2

The Raman spectrum of crystalline SiSe_2 has not been reported or analyzed in detail. The known crystal structure allows nine Raman active modes distributed among four symmetry species as follows, $2A_g + 3B_{1g} + 2B_{2g} + 2B_{3g}$. The corresponding symmetry coordinates, which represent the simplest representation of atomic motions in the lattice, are shown in Fig. 2(a). The Raman spectrum, obtained from a small fibrous crystal of SiSe_2 , produced by slow cooling of a melt having a nominal composition $x=0.333$ followed by a thermal soak at 960°C , is given in Fig. 5. Equivalent spectra were obtained from other preparations involving recrystallization from melts of initial compositions $x=0.333$ and 0.345 . Frequencies and assignments of the spectrum are given in Table II.

The spectrum of Fig. 5 shows 13 Raman bands of which nine, as expected on the basis of group theory, are prominent. Four very weak bands, attributable to sum or difference combinations, are readily assigned on the basis of the assignments of the nine fundamental modes of Fig. 2(a).

Individual assignments are made as follows. Edge-sharing chains of (SiSe_4) tetrahedra can, as a first approximation, be thought of as molecular SiBr_4 units linked together via extra silicon atoms between the molecules such that tetrahedral coordination at silicon is maintained. The Br (Se) atoms bridge the silicon atoms with a

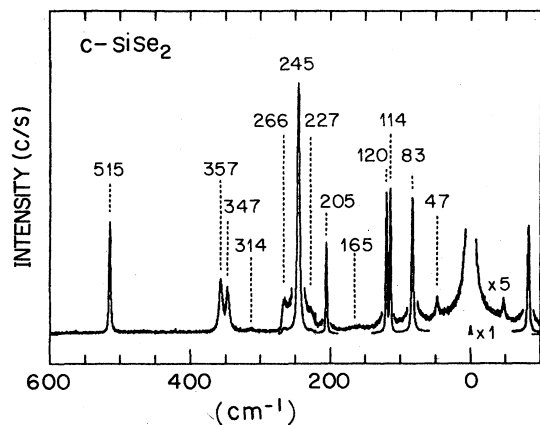


FIG. 5. Raman spectrum of crystalline SiSe_2 . Experimental parameters: excitation (647.1 nm) 240 mW; counting time/step, 0.75 s; scan step size, 0.2 cm^{-1} ; spectral slit width, 2.9 cm^{-1} ; sample temperature 25°C ; signal intensity ($\times 1$) 20000 c/s full scale. Polarization HV.

Si—Br—Si angle near 90°C . One considers the effect of these operations on the vibrational Raman spectrum of the basic SiBr_4 species.³⁶ The frequency of the ν_1 , (a_1) totally symmetric stretching mode of SiBr_4 at 247 cm^{-1} will not shift appreciably so that a band near 247 cm^{-1} is expected. The triply degenerate stretching $\nu_3(f_2)$ mode of SiBr_4 at 494 cm^{-1} will likely be affected significantly because of the constraints imposed on the motions of the Br (Se) atoms by the bridging operation. The remaining deformation modes $\nu_2(e)$ and $\nu_4(f_2)$ of SiBr_4 at 84.8 and

133.6 cm^{-1} are bending coordinates and as such their frequencies should also be affected by bridging. Thus, there is an expected correlation between the spectra observed in SiBr_4 liquid and some of the Raman bands of crystalline SiSe_2 .

The very intense and narrow band at 245 cm^{-1} in the spectrum of $c\text{-SiSe}_2$ can be assigned to the ν_1 , A_g symmetry coordinate of Fig. 2. The other A_g mode, ν_2 , which is a bending coordinate with motional characteristics similar to that of $\nu_2(e)$ of SiBr_4 at 84.8 cm^{-1} , can then be assigned to the single band at 83 cm^{-1} . The $\nu_3(f_2)$ mode of SiBr_4 at 494 cm^{-1} converts in an orthorhombic bridge structure into two modes more or less identified with motions of the silicon atoms transverse to the axes of the chains. The two modes should have comparable energies. Therefore, the two bands at 357 and 347 cm^{-1} in the spectrum of the crystal are assigned as ν_6 , B_{2g} and ν_8 , B_{3g} . By similar arguments the doublet at 120 and 114 cm^{-1} in the spectrum of the crystal are assigned as ν_9 , B_{3g} and ν_7 , B_{2g} respectively. The corresponding $\nu_4(f_2)$ mode of SiBr_4 occurs at 133.6 cm^{-1} so that the effect of bridging is a substantial downward shift in energy.

The four assignments of the B_{2g} and B_{3g} modes under discussion are not definitive in the following sense. Normally one can distinguish the various modes and their symmetry species by standard oriented crystal polarization measurements. In the present case, however, irradiation of the sample is done through two curved glass tubes, one of which has an extremely rough surface which tends to scramble the polarization of the incident light. Secondly, the sample is an ensemble of crystalline fibers radiating

TABLE II. Raman spectrum of crystalline SiSe_2 and $\text{Si}_x\text{Se}_{1-x}$ glasses.

Frequency (cm^{-1})	$c\text{-SiSe}_2$ Relative intensity ^a	Assignment ^b	$g\text{-Si}_x\text{Se}_{1-x}$ Frequency (cm^{-1})	
			$x=0.333$	0.400^c
515	89	ν_3 , B_{1g}	521 470	520 445
357	42	ν_6 , B_{2g}	380	380
347	35	ν_8 , B_{3g}	358	358
314	~ 2	$\nu_4 + \nu_7 = 319$, B_{3g}	303	286
266	23	$\nu_8 - \nu_2 = 264$, B_{3g}		
245	1000	ν_1 , A_g	245 236	235
227	16	$\nu_8 - \nu_9 = 227$, A_g		
205	360	ν_4 , B_{1g}	218 202 193 164	215 200 184 170
165	~ 2	$\nu_5 + \nu_9 = 167$, B_{2g}		
120	560	ν_9 , B_{3g}	131	131
114	580	ν_7 , B_{2g}		
83	530	ν_2 , A_g	70	70
47	16	ν_5 , B_{1g}	9	18

^aHorizontal-vertical polarization.

^bMode numbering is in the Herzberg notation.

^cText and Fig. 10 give values and assignments for other values of x .

from a common point and one tries to irradiate as small a number of these fibers as possible. This is clearly not possible nor is it practical to remove some of these crystals from the confines of the sample tube without compromising their chemical integrity. Nevertheless, it was possible to confirm via polarization measurements that the two bands at 357 and 114 cm^{-1} are of the same symmetry species, as are the two bands at 347 and 120 cm^{-1} . The assignments of these pairs to the B_{2g} and B_{3g} species, respectively, were made by qualitative estimation of force constants in each case.

Different kinds of arguments are required for the remaining three symmetry coordinates. The LO-TO modes of elemental silicon occur at about 522 cm^{-1} (Ref. 37) and there is no analog of this mode in $c\text{-SiSe}_2$. There is a ν_3 symmetry coordinate, however, in which the silicon atoms in the chains along the edges of the unit cell parallel to the c axis move coherently along that axis. Concurrently, the silicon atoms in the chain through the center of the unit cell move along the same axis but in a direction 180° from that of the silicon atoms in the cell-edge chains. Because of the presence of the bridging selenium atoms, the forces opposing the motion of the comparatively light silicon atoms will be high and therefore a reasonably high frequency might be expected. The relatively isolated band observed at 515 cm^{-1} is a reasonable candidate for assignment as the ν_3 , B_{1g} symmetry coordinate of Fig. 2. The ν_5 , B_{1g} mode is essentially a torsion motion of individual chains and such modes normally represent low-energy vibrations and are also often of low Raman intensity. Accordingly, the weak band at 47 cm^{-1} is a strong candidate for assignment of ν_5 .

The final symmetry coordinate, ν_4 , B_{1g} , would then belong to the narrow Raman band at 205 cm^{-1} . The atomic motions in this coordinate are a scissorslike motion involving both bond-stretching and angle-bending motions.

There are four additional very weak bands that can be interpreted in more than one way. First, these bands at 314 , 266 , 227 , and 165 cm^{-1} may arise from a crystal-defect-induced relaxation of the selection rules which would allow observation of formally Raman-forbidden but infrared-active modes. Alternatively, allowed two-phonon processes are attractive, are more defensible, and do not require using unknown or unavailable data. The assignments to two sum bands and two difference bands along with the resulting symmetry species are listed in Table II. The frequency agreements, as expected and required for difference bands,³⁸ are very good. Frequency comparisons for sum bands are reasonable in view of the extremely low amplitudes of the signals and the large bandwidths. The anharmonicity corrections are positive.

B. SiSe_2 glass

Silicon selenide glasses $\text{Si}_x\text{Se}_{1-x}$ covering the composition range $0.333 \leq x \leq 0.400$ were examined in their as-prepared state. To emphasize specific features in their Raman spectra various presentations of data are given. Log plots of the scattered intensity versus cm^{-1} tend to emphasize weak bands at the expense of the strong ones. Thus, Figs. 6 and 7 show such log plots for vertical-

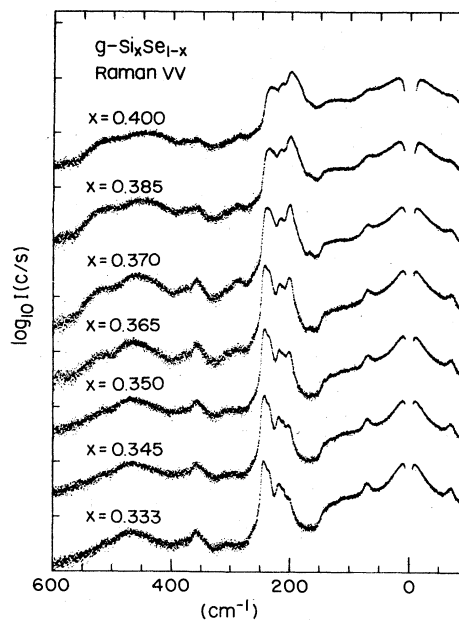


FIG. 6. Raman spectra of $\text{Si}_x\text{Se}_{1-x}$ ($0.333 \leq x \leq 0.400$) glasses. Signal amplitudes in $\log_{10} I$ (c/s). Polarization VV. Experimental parameters: excitation (647.1 nm) 200 mW except for $x=0.365$ where $P=150\text{ mW}$; spectral slit width 1.9 cm^{-1} except for $x=0.365$ where it is 2.4 cm^{-1} ; stepping increment, 0.2 cm^{-1} ; counting time (bottom to top in seconds) 0.75 , 0.5 , 1.0 , 0.6 , 0.5 , 0.75 , and 1.0 . Signal amplitudes of strongest peaks are in the range $3300\text{--}6100\text{ c/s}$.

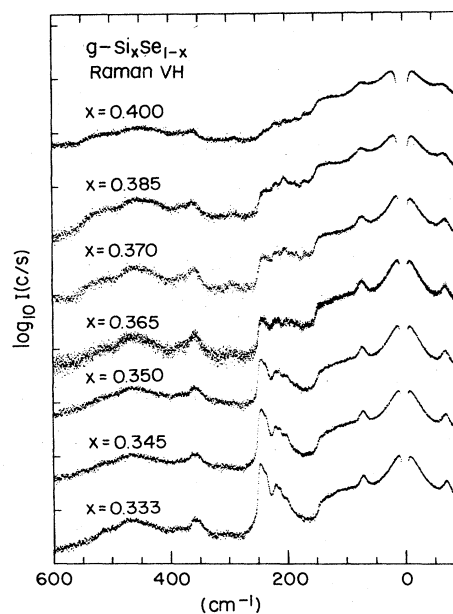


FIG. 7. Raman spectra of $\text{Si}_x\text{Se}_{1-x}$ glasses. Polarization VH. Presentation and experimental parameters are the same as in Fig. 6 except for step size, 0.4 cm^{-1} (0.2 cm^{-1} for $x=0.365$); counting time 2.0 s (0.6 s for $x=0.365$). Signal amplitudes of the peak near 245 cm^{-1} are in the range $210\text{--}2350\text{ c/s}$.

vertical (VV) and the corresponding vertical-horizontal (VH) spectra. Figures 8 and 9 show normalized intensity against cm^{-1} plots for the spectral regions 150 to 300 and 0 to 150 cm^{-1} , respectively. This focuses attention on the more prominent bands which will be used to support the CLCC model over the extended-chain and radical-chain alternatives. Furthermore, information relating to the introduction of disorder into a structure with an initial high degree of medium-range order can, in principle, be gleaned from spectra appearing in these figures.

Although the radical-chain and seleno-siliconyl extended-chain models for a stoichiometric SiSe_2 glass are attractive for their conceptual and structural simplicity, they are not supportable by experimental evidence. The lack of high spin density in SiSe_2 glasses¹⁵ precludes accepting an extended-chain model with sites having unpaired electrons. One could propose that a given chain might terminate with an orbital containing two electrons of paired spin while a neighboring chain would terminate with an empty orbital. The lack of a high spin density would not conflict with such a chain model and the seleno-siliconyl extended-chain model would differ only in the method by which the chains are terminated. This has important consequences and one may look to the observed Raman spectrum for evidence in support of such structures.

If the structure of the glass is dominated by long chains of edge-sharing (SiSe_4) tetrahedra, as has been claimed recently,¹⁷ one should expect close similarities between spectra of the stoichiometric glass and the crystalline compound. Orientational chain disorder would broaden crystalline bands but probably would not cause large frequency shifts. This is expected behavior in noncrystalline solids and liquids in which the $k=0$ selection rule for crystals is relaxed. Any such shifts or the appearance of new bands at significantly different frequencies would

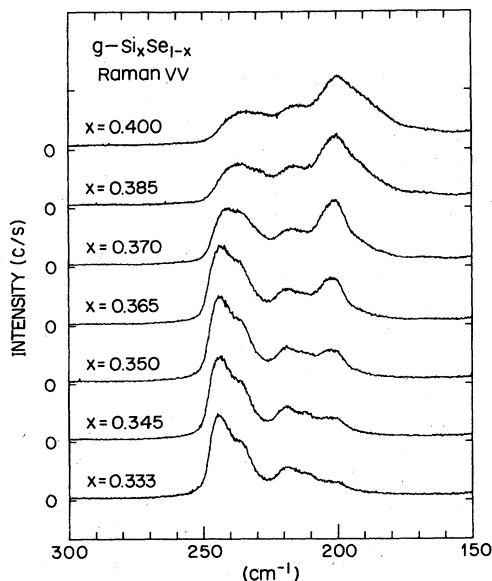


FIG. 8. Raman spectra (linear in c/s) of $\text{Si}_x\text{Se}_{1-x}$ glasses. Polarization VV. Experimental parameters are the same as in Fig. 6.

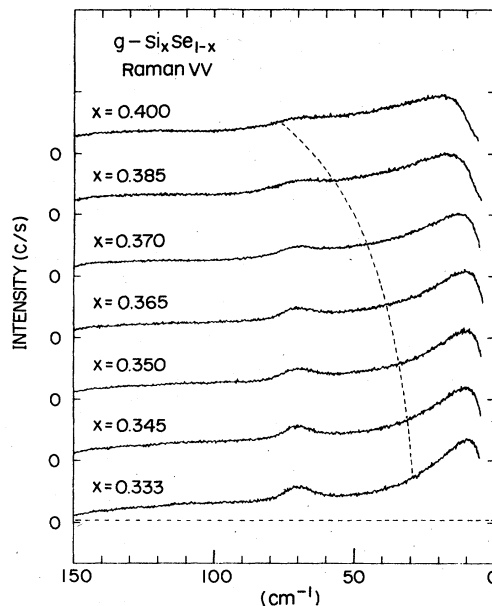


FIG. 9. Raman spectra (linear in c/s) of $\text{Si}_x\text{Se}_{1-x}$ glasses. Polarization VV. Experimental parameters are the same as in Fig. 6. Dashed curve tracks the half-amplitude points of the Bose peaks.

more likely reflect changes in bonding. Therefore, for the extended-chain models to be acceptable, the observed spectrum of the stoichiometric glass should be similar to that of the crystal with the addition of a low-frequency peak typical of glasses and the possible detection of a narrow band arising from terminating seleno-siliconyl groups. The individual bands are expected to be broader than those observed for the crystalline phase.

The data in Figs. 6–9 cannot support either of the extended-chain models. The spectra are far too complex. Figure 8, for example, shows four or five bands in the 190 to 260 cm^{-1} region where only two modes, ν_1 and ν_4 , exist in the spectrum of the crystal. Five bands in the region 300–600 cm^{-1} , all of which are extremely broad, appear in the spectrum of the glass (Figs. 6 and 7). In the spectrum of the crystal, one closely-spaced doublet and a single narrow band appear. The frequency shifts between the two states of matter are also considerable.

At low frequencies, a prominent peak is evident, as expected. The weak 47- cm^{-1} peak of the crystal disappears or is masked by the low-frequency peak and the remaining crystalline bands at 83, 114, and 120 cm^{-1} broaden and undergo some frequency shifts. The low-frequency bands as such are not particularly model dependent. Later in this work the importance of the low-frequency peak as a probe of structural disorder will become more obvious. As an alternative to the unlinked chain models discussed above, it is appropriate to consider in detail the cross-linked chain-cluster model of Fig. 4(a).

The CLCC model contains a number of individual chains of edge-sharing tetrahedra only three of which are shown in Fig. 4(a). The spectra, therefore, should contain bands reminiscent of the crystal. In addition, corner-sharing (SiSe_4) tetrahedra are used to bridge individual

chains. The observed spectra ought to reflect these structural elements which are arranged in a coherent fashion resulting in clusters with complete short-range order and substantial medium-range order.

The bands in Figs. 6–9 at 245 and 202 cm^{-1} correspond to the totally symmetric (SiSe_4) stretching mode and to the scissoring mode of the crystal at 245 and 205 cm^{-1} , respectively. Such bands do not distinguish between the extended-chain models and the CLCC model; they simply support the idea that edge-sharing tetrahedral chains are an integral part of the real glass. The appearance of bands at 236, 218, and possibly at 193 cm^{-1} in the glass spectra support the idea of corner-sharing tetrahedra predicted solely by the CLCC model. This is the region expected for Si-Se corner-sharing stretching modes.

The higher-frequency region is also of interest. The 515- cm^{-1} band in the crystal represents the concerted motion of the silicon atoms along the chains. This mode loses its significance in extended-chain models because the chains are no longer required to retain their relative parallelism, nor are they necessarily required to behave as rigid rods. Instead, orientational chain disorder is expected as is perhaps a tendency for the chains to coil or bend. In the CLCC model, individual chains are much shorter and chain parallelism is more rigorously maintained. The distance between chain axes will be larger than in the crystal since this distance is determined by the corner-sharing bridging units in the structure. Accordingly, the narrow band 515 cm^{-1} in the crystal should be replaced by a much broader band in the glass for the CLCC model. The weak band at 521 cm^{-1} present in the spectra of Figs. 6 and 7, although barely detectable, is an appropriate candidate.

The presence of edge-sharing chains in all models requires identification of a band or bands corresponding to the 357, 347- cm^{-1} doublet in the spectrum of the crystal. A reasonably prominent band at 358 cm^{-1} and a weak band at 380 cm^{-1} satisfies this obligation. A very broad band centered at about 470 cm^{-1} has no counterpart in the spectrum of the edge-sharing chains in the crystal. Corner-sharing (SiSe_4) tetrahedra linking these chains together, however, should have Raman bands corresponding to Si-Se stretching vibrations of (SiSe_3) and (SiSe_2) bridging structural units.

Comparison values for appropriate vibrational bond-stretching frequencies in FSiBr_3 (Ref. 39) and F_2SiBr_2 (Ref. 40) are $\nu_{\text{sym}}(\text{SiBr}_3)=318 \text{ cm}^{-1}$, $\nu_{\text{asym}}(\text{SiBr}_3)=520 \text{ cm}^{-1}$, $\nu_{\text{sym}}(\text{SiBr}_2)=414 \text{ cm}^{-1}$, and $\nu_{\text{asym}}(\text{SiBr}_2)=540 \text{ cm}^{-1}$. The triply degenerate stretching vibration of the tetrahedrally bonded SiBr_4 molecule occurs at 494 cm^{-1} .³⁶ The broad bands in the spectrum of *g*- SiSe_2 centered near 470 and 521 cm^{-1} can therefore satisfy this aspect of the model. Thus, two kinds of vibrational motion can contribute to the 521- cm^{-1} band, silicon motion in chains, as discussed earlier, and Si-Se motions at corner-sharing sites. By these arguments, the weak band at 303 cm^{-1} would correspond to the band observed at 318 cm^{-1} in molecules containing (SiBr_3)-type structural entities.

Regarding the glass spectrum for $x=0.333$ alone, the lowest-frequency region from 0 to 150 cm^{-1} does not give information especially important for direct interpretation

in terms of the glass structure. That kind of information can be extracted from the series of spectra ($0.333 < x < 0.400$) as discussed in the next section. The spectrum of the stoichiometric SiSe_2 glass shows only two vibrational bands at 131 and 70 cm^{-1} . Both, which appear in Figs. 6, 7, and 9, are broad as expected. The extreme breadth of the 131- cm^{-1} band might be used to favor the CLCC model, but realistically the frequencies, band contours, and the changes that occur on introducing corner-sharing units into the structure are not expected to be model dependent.

The appearance of a broad low-frequency peak (Fig. 9) confirms only that the sample is indeed a glass. Further information about the internal structure of the glass may be extracted by considering the series of spectra for $0.333 < x < 0.400$. This is discussed in the next two subsections.

C. Variable composition $\text{Si}_x\text{Se}_{1-x}$ glasses

The cross-linked chain-cluster model of SiSe_2 glasses is more consistent with available evidence than either of the simplistic extended-chain models. Moreover, the CLCC model has attractive structural features which lend themselves to the incorporation of additional silicon atoms, or equivalently the removal of selenium atoms, up to and including the composition $x=0.40$. This is a natural cutoff point favoring glass formation. Beyond that cutoff, further additions of silicon or removal of selenium must proceed by a different mechanism.

The spectral changes that accompany structural modifications in the glass are best considered by focusing on various spectral regions. In the discussion that follows, the idea of using group frequencies to describe structural units has considerable merit.

As discussed earlier, the region above 300 cm^{-1} contains bands that arise mainly from antisymmetric vibrational motions in (SiSe_4) tetrahedra that would otherwise be degenerate if the tetrahedra were isolated. Since they are not isolated, the observed bands should be broad and there should be several of them. This is especially true if both edge- and corner-sharing tetrahedra are integral parts of the glass structure. The effect of eliminating selenium atoms is first to decrease both short- and medium-range order by introducing Si-Si bonding. Ultimately pure edge-sharing tetrahedra are eliminated from the structure. At that point, Si-Si dumbbells link face-sharing tetrahedra. All of these effects will shift Si-Se-Si bond angles from near 80° in edge-sharing situations⁸ to values closer to the normal tetrahedral angle of 109° 28'. This, in turn, will have a significant effect on depolarization ratios, especially for those vibrational modes corresponding to totally symmetric modes in isolated tetrahedra.

Figures 6 and 7 show the evolution of the complete spectra in the composition range $0.333 < x < 0.400$. In the region from about 280 to 600 cm^{-1} the spectra change very little. The frequency of the band at 521 cm^{-1} is virtually invariant with composition although its amplitude increases slightly with increasing silicon concentration. This band by virtue of its behavior and its apparent coincidence with the frequency of a Si-Si vibrational mode in

elemental silicon and the ν_3 , B_{1g} mode c - SiSe_2 , may represent a measure of Si-Si bonding in the $\text{Si}_x\text{Se}_{1-x}$ glasses.

Vibrational modes more directly related to motions of selenium atoms appear at 470, 380, 358, and 303 cm^{-1} . The frequencies of two of these decrease markedly as a function of composition. These bands, initially at 470 and 303 cm^{-1} have no counterpart in the spectrum of pure crystalline SiSe_2 . Beside their decrease in frequencies with decreasing Se content, their relative amplitudes, which appear to reach a maximum at $x=0.37$, and their bandwidths, which are broadest at $x=0.40$, monitor the deterioration of medium-range order as the compositions move away from SiSe_2 . The frequency changes with composition are easier to visualize in the plot shown in Fig. 10.

The region from about 150 to 290 cm^{-1} shows other dramatic effects as well. This is the frequency range in which the vibrational motions are derived from symmetric modes in analogous isolated molecules of the type $\text{Si}Y_mZ_{4-m}$ where $0 \leq m \leq 4$. Figures 6, 7, 8, and 10 show that the band originating at 245 cm^{-1} , and which is identified with a stretching mode in edge-sharing tetrahedra, systematically shifts down in frequency and relative amplitude with decreasing selenium content until it is indistinguishable from the frequency invariant mode at 236 cm^{-1} . The latter has already been assigned to a stretching mode for a tetrahedral corner-sharing unit in the stoichiometric glass structure. Coincident with these changes is a gradual decrease in the depolarization ratio of all of the bands in this region as edge-sharing tetrahedra are replaced with corner-sharing and face-sharing structural entities. In other words, relaxation of the 80° Si-Se-Si angle restraint of edge-sharing tetrahedra to near-normal tetrahedral angles is accompanied by a marked decrease in the depolarization ratio.

Another notable feature in the spectra of Fig. 8, but less obvious in Figs. 6 and 7, is the appearance of a very weak band at 193 cm^{-1} at compositions of $x \geq 0.345$. Its amplitude increases with x and its frequency decreases significantly. Coincident with the growth of this mode is the

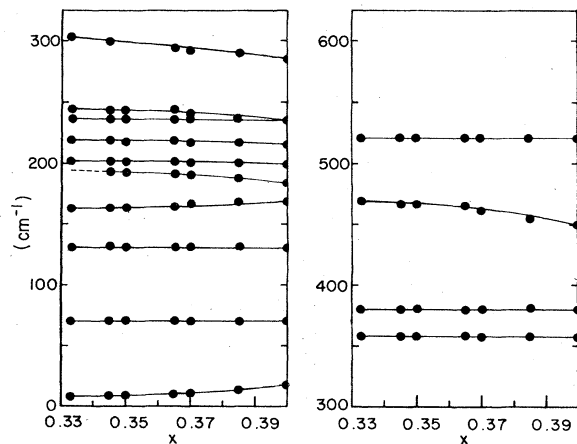


FIG. 10. Frequency dispersion of the peak frequencies of bands as a function of x in $\text{Si}_x\text{Se}_{1-x}$ glasses.

appearance of another at 164 cm^{-1} , whose frequency increases with x to 170 cm^{-1} . The frequencies of these two modes approach each other as x approaches the limiting value of 0.4 (Fig. 10). Thus, although one cannot realistically assign these two bands in terms of particular atomic motions, it is apparent that as medium-range disorder increases, the nature of the motions approaches equivalence. The prominent band at 218 cm^{-1} changes very little with x , and therefore supports our view that it represents a measure of non-edge-sharing motions present initially at $x=0.333$ and which are retained as x approaches 0.4.

The two low-frequency bands at 131 and 70 cm^{-1} are not affected a great deal by changes in x as discussed earlier. The atomic motions giving rise to these broad Raman bands are very complex and mask subtle changes in the structure. The low-frequency peak, however, is much more interesting.

D. The low-frequency peak

The low-frequency peak, unlike those bands appearing at higher frequencies, cannot be identified in terms of specific symmetry or normal coordinates. Rather, it arises from collective motions in materials lacking long-range three-dimensional order and includes acoustic relaxation processes. To date, one cannot predict the peak in the frequency distribution nor the overall width of the band. The $\text{Si}_x\text{Se}_{1-x}$ system is particularly interesting in this regard because both the peak in the frequency spectrum and the width of the band increase systematically with the interruption of medium-range order in the structure of the glass material. As we have seen in earlier sections, introduction of silicon atoms into SiSe_2 contributes to this decrease in medium-range order. Figure 9 illustrates the evolution of the peak as a function of x . The bandwidth represented by the dashed curve was arbitrarily selected as the point at which the peak signal amplitude has fallen to half its value. Figure 11 shows the variation of the peak frequency with x .

The composition range of interest extends from $x=0.333$ to 0.4, or SiSe_2 to Si_2Se_3 . According to our model, the removal of selenium from the relatively ordered structure first has the effect of introducing a discontinuity from one region of edge-sharing tetrahedra to the next via corner-sharing bridging. With continued removal of selenium, chain lengths must become shorter and the relative proportion of the structure maintaining medium-range order must decrease. Thus, the rate at which the structure can dissipate its internal energy via collective mode relaxation increases. The net effect is to broaden the band (in frequency space) associated with collective motions.

The frequency of maximum amplitude of the low-frequency peak is related in a qualitative way with the size of units having highly ordered structures. In the limit of complete three-dimensional ordering, the frequency goes to zero as does the amplitude. Therefore, one reasonably expects the peak frequency to be a measure of the degree of order or disorder in the system. Accordingly, as selenium is removed, medium-range order decreases and the frequency of the peak increases. The effect is dramati-

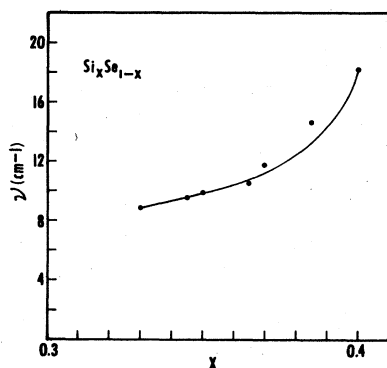


FIG. 11. Expanded version of the low-frequency peak-frequency dispersion in $\text{Si}_x\text{Se}_{1-x}$ glasses.

ly evident in Fig. 11, where ν_{peak} changes by a factor of 2 as x changes from 0.333 to 0.4. The change is most rapid as x approaches 0.4, the region in which edge-sharing tetrahedra are being destroyed at the highest rate.

There is little literature available that is comparable to the present work where systematic changes in local order are monitored via the low-frequency peak. The most relevant studies were done with $\text{Ge}_y\text{Se}_{1-y}$ and $\text{Ge}_y\text{S}_{1-y}$ which deal with compositions on the germanium-rich side of the stoichiometric $y=0.333$ compound. The work of Lucovsky, Nemanich, and Galeener contains information of particular interest.⁴¹ The three compositions for which data are given include GeSe_2 ($y=0.333$), Ge_2Se_3 ($y=0.400$), and Ge_3Se_4 ($y=0.429$), as well as the three sulfur analogs. As y increases, and presumably since the GeSe_2 composition has the greatest degree of medium-range order, the low-frequency peak frequencies increase substantially. The work of Nemanich, Solin, and Lucovsky⁴² does not lend itself to comparison. That of Kawamura and Matsumura,⁴³ although it covers a very large range of composition, is incomplete in the frequency region below 100 cm^{-1} .

In his early work Nemanich⁴⁴ studied the low-frequency peak and analyzed it in terms of acoustic processes in a homogeneous amorphous medium. Agreement with theory is excellent up to and including the low-frequency peak frequency. At $\nu > \nu_{\text{peak}}$, there is only poor agreement and it gets worse as ν increases. Kawamura *et al.*,⁴⁵ on the other hand, invoke a different mechanism in their study of arsenic sulfide glasses. They claim that the low-frequency peak arises from vibrations of layerlike clusters coupled with each other via van der Waals forces. The processes responsible for the low-frequency peak in

glasses appears to be more complex than one might have expected on the basis of either work. Our own results and conclusions, although qualitative, provide added incentive for a more detailed study of the low-frequency spectral region. This will be reported in due course.⁴⁶ In the meantime, our data show the effect on the low-frequency peak of systematically interrupting the medium-range order in glasses, a structural consideration that has not been evaluated in the most recent treatment of the problem.⁴⁷

VII. CONCLUSIONS

In contrast to an earlier claim¹⁷ that stoichiometric SiSe_2 glass is "composed of extended chains of edge-sharing tetrahedra with the composition of the molecular clusters being the same as the crystalline compound," the present work demonstrates convincingly that such a conclusion is a gross oversimplification. The structure is clearly much more complex. It includes both edge- and corner-sharing (SiSe_4) tetrahedra. The model, developed here, contains both entities and provides a basis for the formation of continuous range of glasses covering compositions from SiSe_2 and Si_2Se_3 ($0.333 \leq x \leq 0.400$). All of the Raman spectral data support this model and is inconsistent with any of the extended-chain models. Of special importance in this regard is the spectral evidence for both corner- and edge-sharing tetrahedra, the growth of the former at the expense of the latter as x increases from 0.333 to 0.4 in $\text{Si}_x\text{Se}_{1-x}$ and the utility of information presented by the low-frequency peak for tracking these structural changes. Thus, the CLCC model appears to have considerably more merit than any of the chain-only models now extant. Moreover, by virtue of the similarities between $c\text{-SiSe}_2$ and $c\text{-SiS}_2$, similar conclusions are probably valid for $\text{Si}_x\text{S}_{1-x}$ glasses as well.

Note added in proof. After submission of this paper for publication, another Brief Report appeared (Ref. 48) discussing some of the same subject matter contained in the present work. The authors of Ref. 48 appear to be modifying their earlier interpretation in Ref. 17 to approach more closely that presented in considerably more detail here.

ACKNOWLEDGMENTS

We are grateful to Dr. J. C. Phillips for useful discussions in the formative stages of this work and to Dr. H. Schonhorn for valuable comments on the physical properties of organic polymers.

¹G. Dittmar and H. Schafer, *Acta Crystallogr. Sect. B* **32**, 2726 (1976).

²Parentheses are used to indicate linked tetrahedra as opposed to isolated molecular units.

³E. Zintl and K. Loosen, *Z. Phys. Chem. (Leipzig)* **174**, 301 (1935).

⁴A. Weiss and A. Weiss, *Z. Naturforsch.* **7B**, 483 (1952).

⁵A. Weiss and A. Weiss, *Z. Anorg. Allg. Chem.* **276**, 95 (1954).

⁶J. Cueilleron and R. Hillel, *Bull. Soc. Chim. Fr.* **1967** (8), 2973 (1967).

⁷R. Hillel and J. Cueilleron, *Bull. Soc. Chim. Fr.* **1971** (2), 394 (1971).

⁸J. Peters and B. Krebs, *Acta Crystallogr. Sect. B* **38**, 1270 (1982).

⁹R. Azoulay, H. Thibierge, and A. Brenac, *J. Non-Cryst. Solids* **18**, 33 (1975).

- ¹⁰J. C. Phillips, *J. Non-Cryst. Solids* **34**, 153 (1979), and references cited therein.
- ¹¹J. E. Griffiths, G. P. Espinosa, J. P. Remeika, and J. C. Phillips, *Phys. Rev. B* **25**, 1272 (1982), and references cited therein.
- ¹²P. Boolchand, J. Grothaus, W. J. Bresser, and P. Suranyi, *Phys. Rev. B* **25**, 2975 (1982), and references cited therein.
- ¹³J. E. Griffiths, G. P. Espinosa, J. C. Phillips, and J. P. Remeika, *Phys. Rev. B* **28**, 4444 (1983).
- ¹⁴H. Gabriel and C. Alvarez-Tostado, *J. Am. Chem. Soc.* **74**, 262 (1952).
- ¹⁵H. H. Emons and L. Theisen, *Z. Anorg. Allg. Chem.* **361**, 321 (1968).
- ¹⁶A. Weiss and A. Weiss, *Z. Naturforsch* **8B**, 104 (1953).
- ¹⁷M. Tenhover, M. A. Hazle, and R. K. Grasselli, *Phys. Rev. Lett.* **51**, 404 (1983); M. Tenhover, M. A. Hazle, R. K. Grasselli, and C. W. Thompson, *Phys. Rev. B* **28**, 4608 (1983).
- ¹⁸E. A. Hauschild and C. R. Kannewurf, *J. Phys. Chem. Solids* **30**, 353 (1969).
- ¹⁹D. L. Rousseau, R. P. Bauman, and S. P. S. Porto, *J. Raman Spectrosc.* **10**, 253 (1981).
- ²⁰*Handbook of Chemistry and Physics*, 43rd edition, edited by C. D. Hodgman (Chemical Rubber Publishing Co., Cleveland, 1961), p. 647.
- ²¹N. V. Sidgwick, *The Chemical Elements and Their Compounds* (Oxford University Press, New York, 1950), Vol. II, p. 949.
- ²²P. Tronc, M. Bensoussan, A. Brenac, and C. Sebenne, *Phys. Rev. B* **8**, 5947 (1973), and references cited therein.
- ²³J. Vennik and R. Callaert, *C. R. Acad. Sci.* **260**(2), 496 (1965).
- ²⁴L. G. Bailey, *J. Phys. Chem. Solids* **27**, 1593 (1966).
- ²⁵R. F. Brebick, *J. Chem. Phys.* **49**, 2584 (1968).
- ²⁶T. G. Davey and E. H. Baker, *J. Mat. Sci. Lett.* **15**, 1601 (1980).
- ²⁷Fixative temperature is used here instead of the more common term fictive, because the former carries a connotation of fixing the structure of the material that is present in the melt at that temperature by quenching. That structure, among other things, is a function of temperature. Fictive, on the other hand, carries with it a connotation of some imaginary or fictitious state which in our view is a more nebulous descriptive term.
- ²⁸H. Schnöckel, *Angew. Chem. Int. Ed. Eng.* **19**, 323 (1980).
- ²⁹M. L. Delwaulle and F. Francois, *C. R. Acad. Sci.* **226**, 896 (1948).
- ³⁰M. L. Delwaulle and F. Francois, *C. R. Acad. Sci.* **220**, 817 (1945).
- ³¹D. W. Van Krevelen, *Properties of Polymers* (Elsevier, Amsterdam, 1972), p. 49.
- ³²K. Ploog, W. Stetter, A. Nowitzki, and E. Schönherr, *Mat. Res. Bull.* **11**, 1147 (1976).
- ³³P. E. Gregoriades, G. L. Bleris, and J. Stoemenos, *Acta Crystallogr. Sect. B* **39**, 421 (1983).
- ³⁴F. G. Wakim, A. al-Jassar, and S. A. abo-Namous, *J. Non-Cryst. Solids* **53**, 11 (1982).
- ³⁵J. Hafner, *Phys. Rev. B* **28**, 1734 (1983), and earlier references cited therein.
- ³⁶R. J. H. Clark and P. D. Mitchell, *J. Chem. Soc. Faraday Trans. 2* **71**, 515 (1975).
- ³⁷J. P. Russell, *Appl. Phys. Lett.* **6**, 223 (1965).
- ³⁸G. Herzberg, *Infrared and Raman Spectra of Polyatomic Molecules* (Van Nostrand, Princeton, 1945), Vol. II, p. 269.
- ³⁹J. Goubeau, F. Haenschke, and A. Ruoff, *Z. Anorg. Allg. Chem.* **366**, 113 (1969).
- ⁴⁰M. L. Dubois, M. B. Delhaye, and F. Wallart, *C. R. Acad. Sci. Ser. B* **269**, 260 (1969).
- ⁴¹G. Lucovsky, R. J. Nemanich, and F. L. Galeener, in *Proceedings of the VIIth International Conference on Amorphous and Liquid Semiconductors, Edinburgh, 1977*, edited by W. E. Spear (CICL, University of Edinburgh, Edinburgh, 1977), p. 130.
- ⁴²R. J. Nemanich, S. A. Solin, and G. Lucovsky, *Solid State Commun.* **21**, 273 (1977).
- ⁴³H. Kawamura and M. Matsumura, *Solid State Commun.* **32**, 83 (1979).
- ⁴⁴R. J. Nemanich, *Phys. Rev. B* **16**, 1655 (1977).
- ⁴⁵H. Kawamura, K. Fukumasu, and Y. Hamada, *Solid State Commun.* **43**, 229 (1982).
- ⁴⁶M. Malyj and J. E. Griffiths (unpublished).
- ⁴⁷R. J. Nemanich, *J. Non Cryst. Solids*, **59-60**, 851 (1983).
- ⁴⁸M. Tenhover, R. S. Henderson, D. Lukco, M. A. Hazle, and R. K. Grasselli, *Solid State Commun.* **51**, 455 (1984).